*Physicochem. Probl. Miner. Process., 59(5), 2023, 176950*

http://www.journalssystem.com/ppmp

Physicochemical Problems of Mineral Processing

ISSN 1643-1049


# On the selection of the coarsest size class in flotation rate characterizations

**Francisca Orellana [1], Marcelo Rivera [1], Matías Benítez [1], Karyn Belmonte [1], Luis Vinnett [1, 2]**

[1] Department of Chemical and Environmental Engineering, Universidad Técnica Federico Santa María, Valparaíso 2390123, Chile

[2] Automation and Supervision Centre for Mining Industry, Universidad Técnica Federico Santa María, Valparaíso 2390123, Chile

Corresponding author: luis.vinnett@usm.cl (L. Vinnett)

**Abstract:** This paper studies size-by-size batch flotation kinetics for the separation of Cu at particle sizes +75 µm, investigating the responses in the -150/+75 µm, -212/+150 µm, -300/+212 µm, -355/+300 µm and +355 µm size fractions. The kinetic results were analyzed to identify classes limited by the maximum achievable recovery or low flotation rates. Combinations of these classes were investigated, emulating the selection of the coarsest size in a kinetic study. The impact of compositing size classes was discussed, emphasizing implications in the identification of difficult-to-float components. The -212/+75 µm classes reached steady recoveries at long flotation times, whereas the -355/+212 µm classes presented sustained increasing recoveries at extended flotation times. Flotation rate distributions in the -212/+75 µm classes exhibited mound-shaped distributions, indicating low fractions of rate constants close to zero ($R_\infty$-limited case). Conversely, the -355/+212 µm classes presented reverse J-shaped distributions, with a high fraction of valuable minerals with flotation rates close to zero (rate-limited case). Combining several size classes in the definition of the coarsest size fraction in kinetic characterizations proved to hide the flotation patterns of the less massive constituents (+212 µm classes). The +75 µm and +150 µm cumulative retained classes trended towards steady recoveries, consistently leading to mounded flotation rate distributions. This study highlighted the need for reliable methodologies to select size fractions in kinetic characterizations, as their arbitrary definitions may lead to a misinterpretation of the mineral losses when compositing classes with different flotation responses.

**Keywords:** flotation kinetics, froth flotation, coarse particles, flotation rate distribution

## 1. Introduction

Flotation kinetics plays a critical role in understanding and improving the efficiency of mineral separation processes. Kinetic characterizations allow for the estimation of recovery rates and maximum achievable recoveries from either batch tests or continuous systems (Yianatos *et al.*, 2010; Alvarez-Silva *et al.*, 2016). The analysis of flotation kinetics provides detailed information of the process changes over time. Garcia-Zuñiga (1935) proposed the first kinetic model for batch flotation. Equation (1) expresses the cumulative recovery as a function of time, $R(t)$, with $R_\infty$ being the maximum recovery and $k$ the flotation rate. This model assumes a first-order system with a deterministic flotation rate. This simplification assumes that all valuable particles behave as a single component, which is only applicable when the differences in particle properties of the floating component are not significant.

$$R(t) = R_\infty[1 - \exp(-k\,t)] \tag{1}$$

Imaizumi and Inoue (1963) generalized the kinetic model of Equation (1), representing all random sub-processes by a probability density function $f(k)$. Thus, a spectrum of flotation rates can be evaluated in Equation (2), which increases the flexibility to fit time-recovery data (Bu et al., 2017b; Polat and Chander, 2000). This spectrum accounts for the heterogeneity of the particle properties, being size the most common particle feature assessed in flotation. Although narrower $f(k)$s are expected when

DOI: 10.37190/ppmp/176950

classifying the feed by a particle property (Polat and Polat, 2023), distributions of flotation rates have also been observed on size-by-size and size-by-association bases (Vinnett et al., 2022).

$$R(t) = R_\infty\left[1 - \int_0^\infty \exp(-k\,t)\,f(k)\,\mathrm{d}k\right] \quad (2)$$

Apart from the deterministic model of Equation (1) and the Rectangular $f(k)$ reported by Huber-Panu et al. (1976), the Gamma $f(k)$ of Equation (3) has commonly been used due to its flexibility and low number of parameters. Within Equation (3), Γ is the Gamma function, and $k_\mathrm{G}$ and $a_\mathrm{G}$ are scale and shape parameters, respectively. This distribution has led to satisfactory results in modeling flotation kinetics for ores with varying particle properties (Woodburn and Loveday, 1965; Yianatos et al., 2010; Kapur and Mehrotra, 1973; Harris and Chakravarti, 1970). The flexibility of a Gamma $f(k)$ comes from the shape parameter, $a_\mathrm{G}$. For $a_\mathrm{G} < 1$ this $f(k)$ corresponds to a reverse J-shaped distribution, for $a_\mathrm{G} = 1$ to an exponential distribution, for $a_\mathrm{G} > 1$ to a mounded distribution, and for $a_G \gg 1$ to a normal distribution. For $a_\mathrm{G} \to \infty$, the deterministic model of Equation (1) is obtained.

$$f(k) = \frac{k^{a_\mathrm{G}-1}}{k_\mathrm{G}^{a_\mathrm{G}}\Gamma(a_\mathrm{G})}\,e^{-\frac{k}{k_\mathrm{G}}} \quad (3)$$

From Equations (2) and (3), the cumulative recovery assuming a Gamma $f(k)$ is given by Equation (4). The flexibility of Equation (4) has proven to be suitable in describing flotation kinetics at batch scale, for both unscreened and size-by-size responses (Vinnett et al., 2020).

$$R(t) = R_\infty\left[1 - \frac{1}{(1+k_\mathrm{G}t)^{a_\mathrm{G}}}\right] \quad (4)$$

Size-by-size flotation kinetics allows for the characterization of the process evolution as a function of time, implicitly assessing the efficiency in the formation of particle-bubble aggregates in different size classes (Crawford and Ralston, 1988; Feng and Aldrich, 1999). The effect of particle size on flotation recoveries has extensively been reported in literature, with the studies reported by Gaudin and Trahar pioneering these characterizations (Gaudin et al., 1931; Trahar, 1981). For fine particles, a decrease in recovery has been observed due to a low probability of collision (Lange et al., 1997). On the other hand, the recovery of coarse particles decreases due to lower degrees of liberation and lower stability of the particle-bubble aggregates (Tao, 2005). Although the erratic performances in fine and coarse classes have consistently been observed, kinetic characterizations in these classes have been conducted by different approaches (Ahmed and Jameson, 1985; Amini et al., 2016; Jameson and Emer, 2019; Polat and Chander, 2000; Vinnett et al., 2020). Size-by-size kinetic characterizations are usually carried out under an arbitrary selection of the respective size fractions, which is critical in the coarser classes due to the high heterogeneity in terms of liberation and association. Particularly, the coarsest fraction is the superposition of several subclasses and thus its selection must be made in such a manner that all these subclasses must present similar behaviors. Otherwise, the kinetic responses will be governed by the more massive subclasses, which are typically the finer (and faster) subfractions.

This paper studies size-by-size flotation kinetics in the +75 μm class for the separation of copper minerals, specifically the -150/+75 μm, -212/+150 μm, -300/+212 μm, -355/+300 μm and +355 μm size fractions. From the kinetic responses and parameters, the size classes limited by the maximum achievable recovery or by low flotation rates are identified. Different combinations of these classes as cumulative retained fractions are analyzed, emulating the selection of the coarsest size class in a kinetic study (e.g., +150 μm, +212 μm). The impact of compositing these classes on the observed kinetic responses and parameters are discussed, and the implications on the identification of difficult-to-float components are remarked.

## 2. Experimental procedure

Crushed samples of a copper ore were used in the kinetic characterizations, with a Cu feed grade of 0.92 ± 0.08%. These samples were homogenized and split into 1 kg batches by a Grinder RSD100 rotatory sample divider (POWTEQ, China). Dry grinding was carried out in a Joy Denver® rod mill (Joy Manufacturing Company, Denver Equipment Division, USA). The grinding times were set at 5.5 and 3.75 min, resulting in P80 = 212 μm and P80 =300 μm, respectively. Figs. 1 and 2 show the size-by-size Cu deporment [Figs. 1(a) and 2(a)] and size-by-size Cu grades [Figs. 1(b) and 2(b)] in the flotation feed for P80 = 212 μm and P80 = 300 μm, respectively. Although the Cu feed grades significantly

decreased in the +150 µm fractions, the relative Cu content in these classes was not negligible, representing approximately 20% of this metal for P80 = 212 µm and approximately 30% for P80 = 300 µm.

The ground product was poured into a 2.7 L EDEMET flotation cell (EDEMET Ltda., Chile). Tap water was added to obtain a solid percentage of 33% w/w, and pH was set and kept at 9.5 by a lime slurry. Hostaflot 18275 (Clariant Mining Solutions, USA) at 22.5 g/ton was used as a collector, with a conditioning time of 5.0 min, whereas Aerofroth 70 (Cytec, USA) at 24 mg/L was used as a frother and conditioned for 2.5 min. The flotation cell was operated at 700 rpm, with a constant air flowrate of 8 L/min. Seven concentrates were sampled at the cumulative flotation times of 0.5, 1.5, 4, 10, 16, 24, and 32 min. All flotation products were filtered and dried at 90°C. Three repetitions were conducted for each experimental condition. However, one test at P80 = 212 um did not fulfil the quality control criterion described by Lotter (1995) and was removed from this study (see Appendix A for the experimental variability).

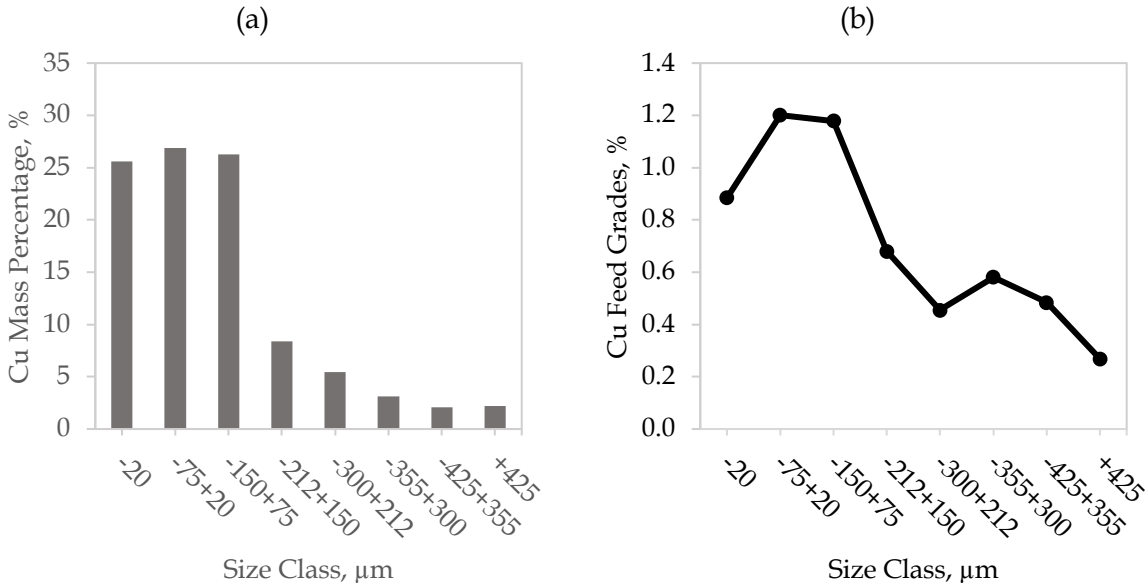


Fig. 1. Size-by-size flotación feed at P80 = 212 µm: (a) Cu deportment; (b) Cu grades

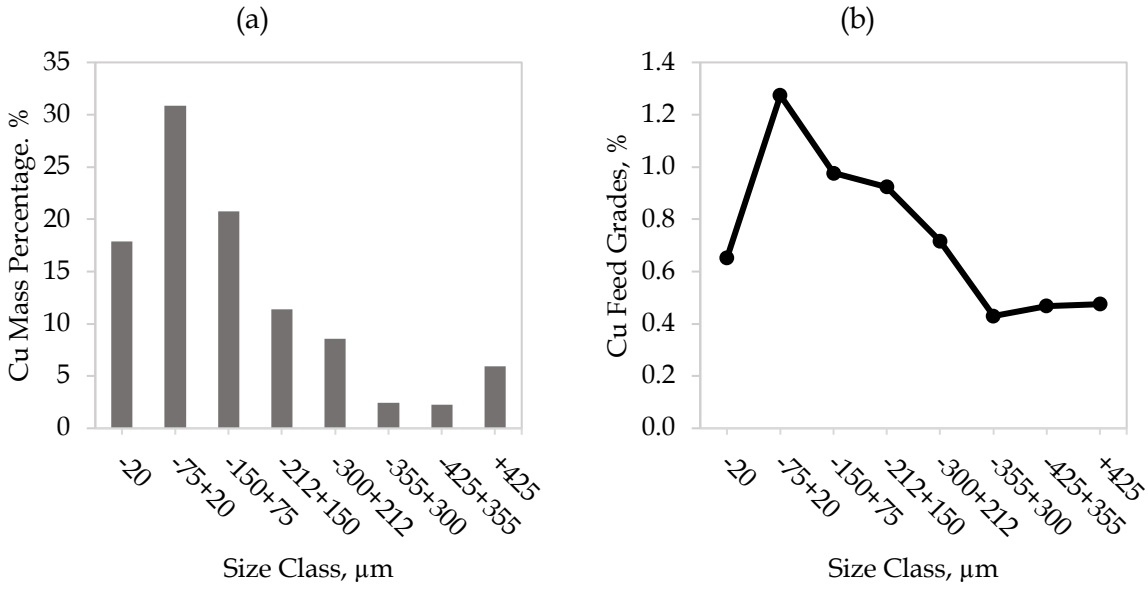


Fig. 2. Size-by-size flotación feed at P80 = 300 µm: (a) Cu deportment; (b) Cu grades

Representative samples from each flotation product were wet screened at 20 μm and dried for 4 hours at 90°C. The +20 μm fraction was then dry screened at 425 μm, 355 μm, 300 μm, 212 μm, 150 μm, 75 μm, and 20 μm. For chemical assaying, the size-by-size feed and products were digested on a hot plate using nitric and perchloric acid (at 150°C), followed by hydrochloric acid (at 200°C). The digested solutions were filtered, diluted, and analyzed by atomic absorption spectrophotometry in the SpectrAA 55 spectrometer (Varian Inc., USA). All size-by-size grades were determined for the studied grinding conditions (P80= 212 μm and P80= 300 μm). From the measured Cu grades and the incremental mass recoveries, data reconciliation was perfomed according to the procedure described by Vinnett et al. (2016). Thus, consistent time-recovery data were obtained for each test.

The kinetic responses were studied in the +75 μm size classes, for both the retained and the cumulative retained size fractions. Thus, the size-by-size flotation kinetics were analysed in the retained classes -150/+75 μm, -212/+150 μm, -300/+212 μm, -355/+300 μm and +355 μm as well as in the cumulative retained classes +75 μm, +150 μm, +212 μm, +300 μm and +355 μm. The latter allowed for the evaluation of arbitrary selections for the coarsest size fraction in kinetic characterizations. The size classes that presented negligible content in all concentrates were removed from the analysis**.**

## 3. Model fitting

The parameters of the Gamma model of Equation (4) were obtained by the least-square estimation (LSE) method of Equation (5):

$$\min \sum_{i=1}^{n} [R_{\text{model}}(t_{\text{i}}) - R_{\text{data}}(t_{\text{i}})]^2 \tag{5}$$

where $R_{\text{model}}$ is the modelled recovery, $R_{\text{data}}$ is the measured recovery, $t_{\text{i}}$ is the i-th flotation time and $n$ is the number datapoints. Equation (5) was implemented in the Optimization Toolbox 8.3 of Matlab (The MathWorks, USA). The estimated $k_{\text{G}}$ and $a_{\text{G}}$ values were used to plot the Gamma $f(k)$s [Equation (3)] and to identify patterns in the flotation rate distributions of the +75 μm size classes.

## 4. Results and discussion

The kinetic responses in the -150/+75 μm, -212/+150 μm, -300/+212 μm and +300 μm size classes were obtained for the condition with P80 = 212 μm. The -355/+300 μm and +355 μm size classes were added for the experimental condition with P80 = 300 μm. To evaluate the impact of defining arbitrary classes as the coarsest fraction, these time-recovery data were combined to obtain the responses in the +75 μm, +150 μm, +212 μm, +300 μm and +355 μm cumulative retained size classes. The latter was only observed for the feed P80 = 300 μm. Fig. 2 presents the size-by-size time-recovery data along with the model fitting for the condition with feed P80 = 212 μm. The Gamma model of Equation (4) was chosen due to its superior performance, in terms of the mean squared error and adjusted $R^2$, with respect to those obtained from classical approaches such as the Single Flotation Rate (García-Zúñiga, 1935) and Rectangular (Huber-Panu, 1976) models (see Appendix B). Fig. 2(a) shows the kinetic results for the retained size classes (-150/+75 μm, -212/+150 μm, -300/+212 μm and +300 μm), whereas Fig. 2(b) presents the responses for the cumulative retained size classes (+75 μm, +150 μm, -+212 μm and +300 μm). Fig. 3 shows the same results for the condition with feed P80 = 300 μm, adding the +355 μm size fraction. From a qualitative analysis of Figs. 2(a) and 3(a) for the retained size-by-size kinetic responses, the -150/+75 μm, -212/+150 μm fractions approximately reached steady recoveries at the end of the process. On the contrary, the coarser fractions -300/+212 μm, -355/+300 μm and +355 μm presented gradual increasing trends at long flotation times. The cumulative retained fractions emulated a selected coarsest size class, Figs. 2(b) and 3(b). In this case, approximately the same pattern was observed, with a trend to obtain steady recoveries in the +75 μm and +150 μm classes. However, these fractions included particles from the -300/+212 μm, -355/+300 um and +355 μm classes, whose sustained increasing trends observed in Figs. 2(a) and 2(b) were almost negligible when combining the size classes.

Table 1 summarizes the differential recoveries at the end of the process for the studied size classes [$\Delta R_{24\text{-}32} = R(t = 32\text{ min}) - R(t = 24\text{ min})$]. At the coarser classes, higher increases in the Cu recoveries were observed in the retained size fractions, which indicated a trend towards rate-limited separations. In the cumulative retained fractions, the classes that incorporates the two finest sizes (-150/+75 μm and -212/+150 μm) presented $\Delta R_{24\text{-}32} < 1.0$. Lower $\Delta R_{24\text{-}3}$ values indicate a trend towards $R_\infty$-limited

separations. The combination of classes with different kinetic responses tended to be controlled by the more massive size fractions, as can be related to the metal deportment shown in Figs. 1 and 2. Thus, some erratic responses in the coarser classes may not be observable when combining a wide range of particle sizes.

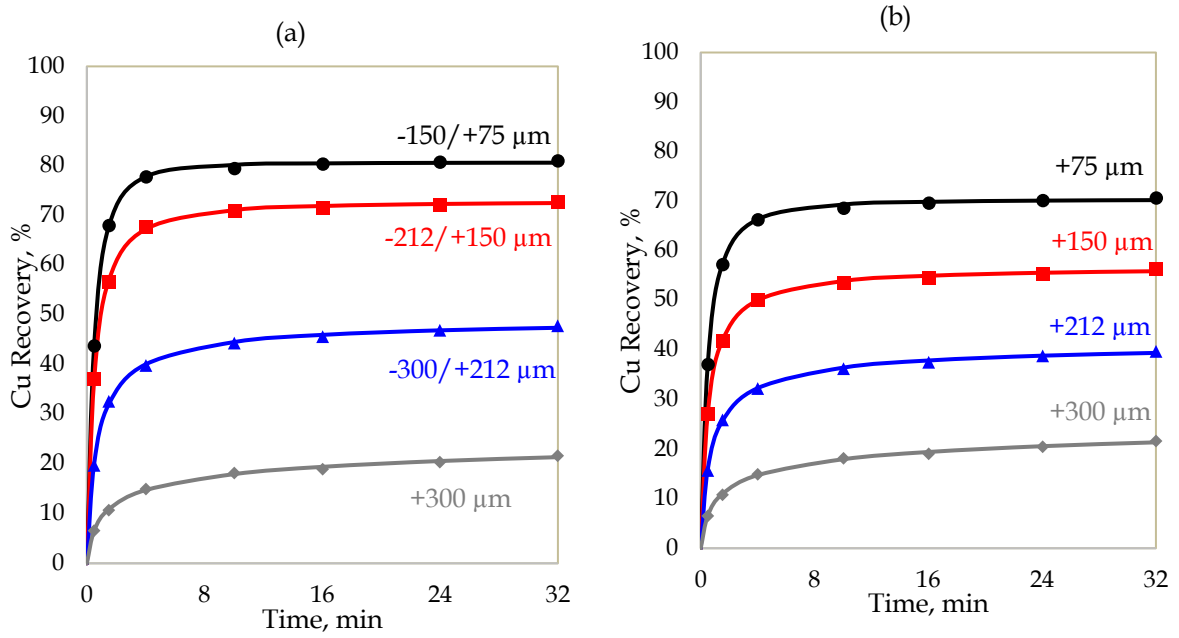


Fig. 3. Size-by-size kinetic responses at feed P80 = 212 µm: (a) retained size classes, (b) cumulative retained size classes that emulate a chosen coarsest class

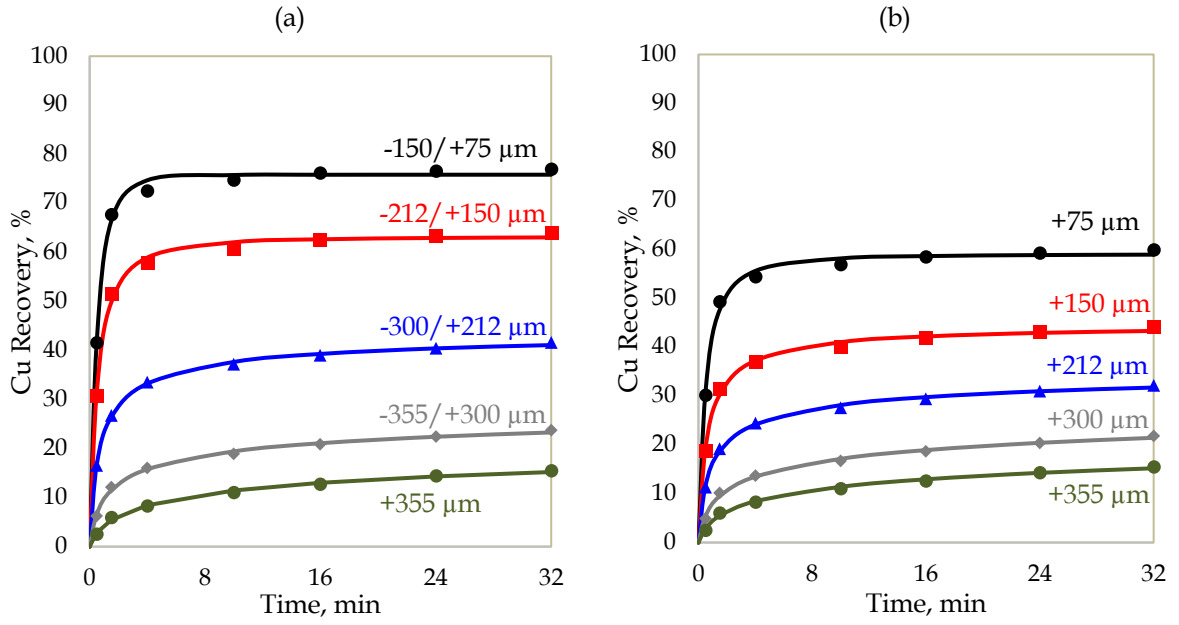


Fig. 4. Size-by-size kinetic responses at feed P80 = 300 µm: (a) retained size classes, (b) cumulative retained size classes that emulate a chosen coarsest class

Figs. 5 and 6 present the estimated flotation rate distributions for the experimental conditions with P80 = 212 µm and P80 = 300 µm, respectively. Figs. 5(a) and 6(a) show the $f(k)$s obtained in the retained size classes, whereas Fig. 5(b) and 6(b) show the $f(k)$s in the cumulative retained fractions. From the former, $f(k)$s in the -150/+75 µm and -212/150 µm size classes presented mound-shaped distributions, which imply a low fraction rate constants close to zero ($k \approx 0$). On the contrary, the incremental size classes +212 µm presented reverse J-shaped distributions, which indicated a significant fraction of rate

Table 1. Differential recoveries at the end of the process for the studied size classes

| Size Class | $\Delta R_{24\text{-}32}$ (Retained) | | Size Class | $\Delta R_{24\text{-}32}$ (Cumulative Retained) | |
|---|---|---|---|---|---|
| | P80 = 212 µm | P80 = 300 µm | | P80 = 212 µm | P80 = 300 µm |
| -150/+75 µm | 0.24 | 0.44 | +75 µm | 0.46 | 0.66 |
| -212/+150 µm | 0.62 | 0.49 | +150 µm | 0.80 | 0.92 |
| -300/+212 µm | 0.90 | 1.20 | +212 µm | 0.99 | 1.22 |
| -355/+300 µm | 1.17 | 1.35 | +300 µm | 1.17 | 1.34 |
| +355 µm | - | 1.06 | +355 µm | - | 1.06 |

constants approaching zero. This fraction justifies the sustained increasing trends in Figs. 3 and 4, as well as the higher $\Delta R_{24\text{-}32}$ values in Table 1 for the +212 µm retained classes. The cumulative retained $f(k)$s shown in Figs. 5(b) and 6(b) proved that the combination of size classes with different recovery patterns led to $f(k)$s governed by the more massive fractions. For example, for the evaluated experimental conditions, the +75 µm size class (combined) was controlled by the results in the -150/+75 µm and -212/150 size µm fractions (see the metal deportment in Figs. 1 and 2). This result indicates that combining too many incremental classes hides internal phenomena related to less massive components. Thus, the flotation patterns in the +212 µm retained fractions at long flotation times were not observed when compositing the +75 µm size class, despite containing more than 10% of the overall valuable metal. Reverse J-shaped distributions indicates a potential to increase the mineral recovery by extending the flotation time (significant fraction of minerals with $k \approx 0$), whereas mound-shaped distributions implies that the process is mainly limited by the maximum recovery (low fraction of minerals with $k \approx 0$). Thus, the combination of several size classes with remarkably different time-recovery trends may lead to misinterpretations of the metal losses. The composited +75 µm size class showed that the slow-rate fractions are negligible and the separation is then $R_\infty$-limited. As more than 20% of this class consisted of +212 µm particles, the combination of a wide range of size classes hid the reverse J-shaped trends in $f(k)$ [and sustained increasing trends in $R(t)$]. Therefore, an arbitrary definition of the coarsest class in kinetic characterizations may distort the $f(k)$ identification. These results highlighted the relevance of defining size classes with similar flotation responses, reducing potential biases when evaluating process efficiencies as a function of particle size.

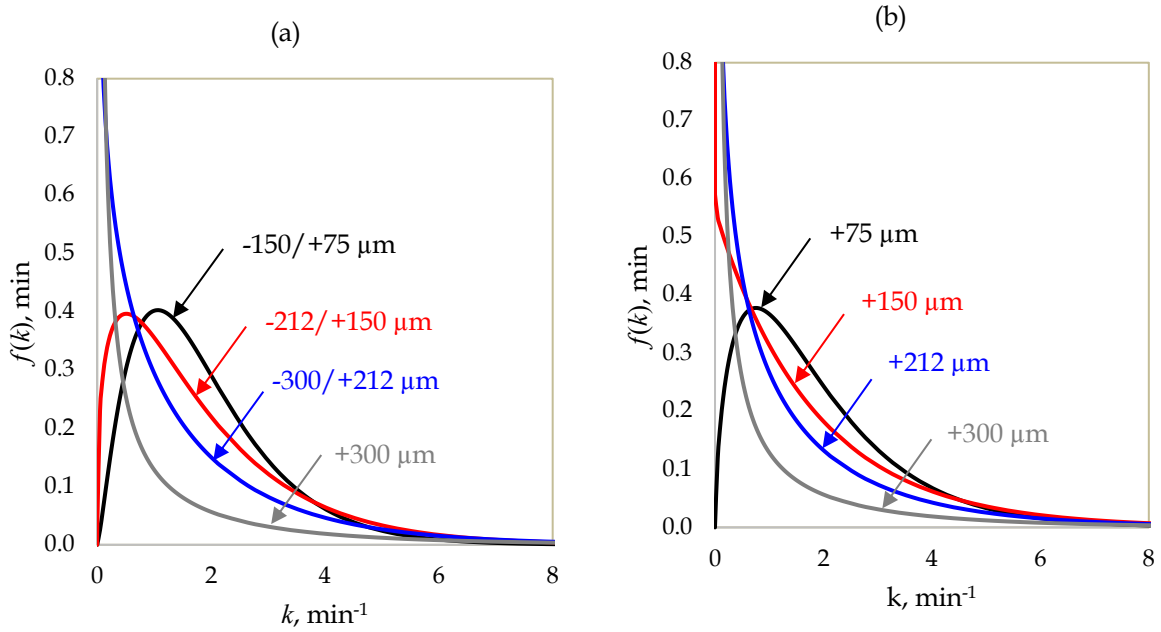


Fig. 5. Size-by-size kinetic flotation rate distributions for a feed P80 = 212 µm: (a) retained size classes, (b) cumulative retained size classes that emulate a chosen coarsest class

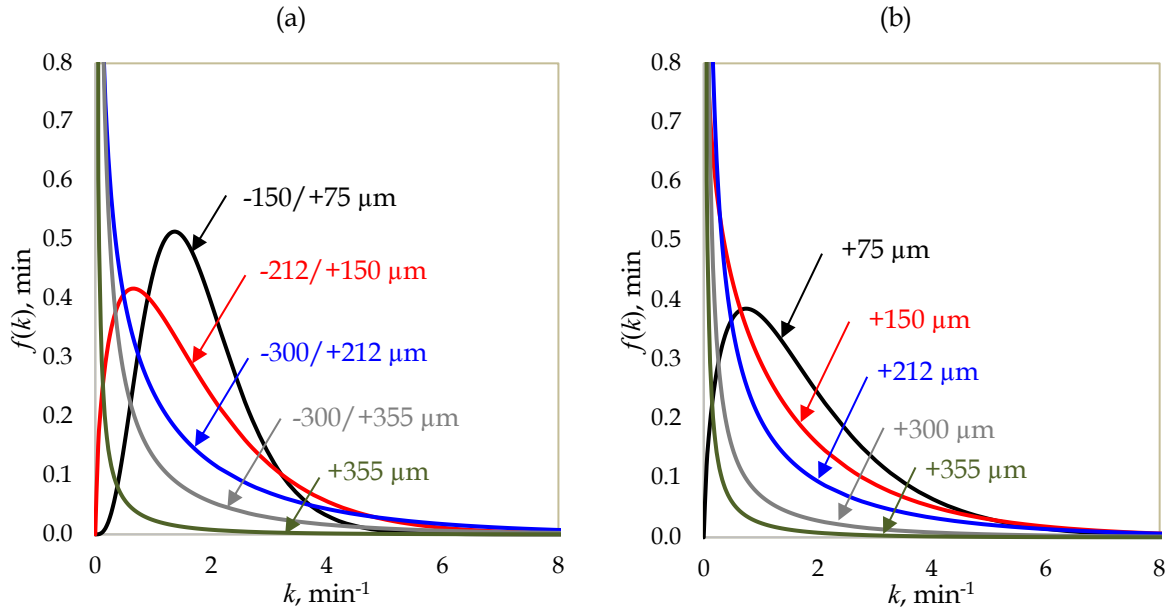


Fig. 6. Size-by-size kinetic flotation rate distributions for a feed P80 = 300 µm: (a) retained size classes, (b) cumulative retained size classes that emulate a chosen coarsest class

The flotation literature on the $f(k)$ patters in the coarser classes has been rather scarce. Bu et al. (2017a) observed a concave trend between the reaction order and particle size in coal flotation. As higher reaction orders are equivalent to reverse J-shaped $f(k)$s in the first-order domain (Vinnett and Waters, 2020), the results reported by Bu et al. (2017a) indicated a trend towards $R_\infty$-limited conditions in the coarser classes. Similar results were obtained by Vinnett et al. (2020) for the batch flotation of galena and chalcopyrite from a complex ore. However, no analyses on the effect of over-grouping the size classes on the fractioned $f(k)$ estimations were performed in these studies. Further developments are being made to define a reliable criterion to select the coarsest size class in a kinetic study, avoiding biases caused by the controlling effect of the more massive size fractions.

## 5. Conclusions

This paper studied the kinetic responses in the +75 µm classes of a batch flotation process, under two experimental conditions. The size-by-size analyses were conducted for the retained and cumulative retained size fraction. The main findings and conclusions are summarized as follows:

- The kinetic responses in the retained size fractions -300/+212 µm, -355/+300 µm, and +355 µm showed gradual increasing trends at long flotation times, whereas the -150/+75 µm, -212/+150 µm size classes reached steady recoveries at the end of the process.
- An analysis of the flotation rate distributions $f(k)$s showed that coarser size classes (+212 µm) presented significant fractions of valuable minerals with rate constants close to zero (reverse J-shaped distributions). These $f(k)$ shapes justified the sustained increasing recoveries at long flotation times. The -212/+75 µm fractions presented mound-shaped distributions, which implied kinetic responses approaching $R_\infty$-limited conditions.
- The combination of several size classes, with different recovery patterns, led to $f(k)$ estimates controlled by the most massive fractions. The cumulative retained +75 µm size class was mostly influenced by the kinetic responses in the -150/+75 µm and -212/150 µm size fractions, given the copper deportment in the feed. Over-combining size classes hid the reverse J-shaped $f(k)$s in the +212 µm classes, which led to a misinterpretation of the metal losses in the coarser fractions.

The interpretation of kinetic results in flotation requires detailed information at specific size fractions, avoiding the combination of size classes with different recovery patterns. As observed in the cumulative retained +75 µm class, the rate-limited conditions in the +212 µm fractions were not observable when combining the kinetic responses, despite the Cu content in these classes represented more than 10% of

the valuable metal. These results highlighted the relevance of defining size classes with similar flotation responses, reducing potential biases when evaluating process efficiencies as a function of particle size.

**Acknowledgments**

Funding for process modelling and control research was provided by ANID, Project Fondecyt 1201335, and Universidad Técnica Federico Santa María, Project PI_LIR_23_02.

**Appendix A**

Tables A1 to A4 presents the experimental recovery data as a function of time for the studied experimental conditions. Tables A1 and A3 shows the results for the retained size classes at P80 = 212 μm and P80 = 300 μm, respectively. Tables A2 and A4 summarizes the same results for the cumulative retained size classes. At P80 = 212 μm the recovery ranges were used a variability indicators, whereas at P80 = 212 μm the sample standard deviations, s, were used as a measure of uncertainty. The variability was higher in the first concentrates and gradually decreased at long flotation times, given the cumulative representation for the Cu recoveries.

Table A1. Size-by-size recovery data and recovery ranges for the retained classes, P80 = 212 μm

| | -150/+75 μm | | -212/+150 μm | | -300/+212 μm | | +300 μm | |
|---|---|---|---|---|---|---|---|---|
| Time, min | Data | Range | Data | Range | Data | Range | Data | Range |
| 0.5 | 42.6, 45.2 | 2.6 | 35.8, 38.5 | 2.8 | 17.8, 21.7 | 3.9 | 5.3, 7.9 | 2.6 |
| 1.5 | 66.4, 69.8 | 3.4 | 54.8, 58,6 | 3.8 | 30.4, 35.0 | 4.6 | 9.7, 11.8 | 2.2 |
| 4.0 | 77.3, 78.3 | 1.0 | 65.2, 70.3 | 5.1 | 37.3, 42.4 | 5.1 | 13.5, 16.3 | 2.8 |
| 10.0 | 78.9, 80.0 | 1.1 | 68.1, 73,6 | 5.5 | 42.5, 46.1 | 3.7 | 17.4, 18.9 | 1.6 |
| 16.0 | 79.8, 81.0 | 0.2 | 68.9, 74.4 | 5.5 | 43.7, 47.6 | 3.9 | 18.2, 19.9 | 1.7 |
| 24.0 | 80.2, 81.4 | 1.2 | 69.5, 75.0 | 5.5 | 44.9, 48.9 | 3.9 | 19.9, 21.0 | 1.1 |
| 32.0 | 80.5, 81.7 | 1.2 | 69.9, 75.7 | 5.8 | 45.9, 49.8 | 3.9 | 21.0, 22.3 | 1.3 |

Table A2. Size-by-size recovery data and recovery ranges for the cumulative retained classes, P80 = 212 μm

| | +75 μm | | +150 μm | | +212 μm | | +300 μm | |
|---|---|---|---|---|---|---|---|---|
| Time, min | Data | Range | Data | Range | Data | Range | Data | Range |
| 0.5 | 35.9, 38.5 | 2.6 | 25.6, 28.7 | 3.1 | 14.1, 17.4 | 3.3 | 5.3, 7.9 | 2.6 |
| 1.5 | 55.9, 58.8 | 2.9 | 40.5, 43.4 | 2.9 | 24.2, 27.8 | 3.6 | 9.7, 11.8 | 2.2 |
| 4.0 | 65.6, 67.1 | 1.5 | 48.8, 51.5 | 2.7 | 30.2, 34.3 | 4.1 | 13.5, 16.3 | 2.8 |
| 10.0 | 68.1, 69.3 | 1.2 | 52.6, 54.7 | 2.1 | 35.0, 37.6 | 2.7 | 17.4, 18.9 | 1.6 |
| 16.0 | 69.0, 70.3 | 1.3 | 53.5, 55.7 | 2.2 | 36.0, 38.9 | 2.9 | 18.2, 19.9 | 1.7 |
| 24.0 | 69.6, 70.9 | 1.3 | 54.5, 56.6 | 2.1 | 37.5, 40.2 | 2.7 | 19.9, 21.0 | 1.1 |
| 32.0 | 70.0, 71.4 | 1.4 | 55.2, 57.5 | 2.3 | 38.4, 41.2 | 2.8 | 21.0, 22.3 | 1.3 |

Table A3. Size-by-size recovery data and recovery ranges for the retained classes, P80 = 300 μm

| | -150/+75 μm | | -212/+150 μm | | -300/+212 μm | | -355/+300 μm | | +355 μm | |
|---|---|---|---|---|---|---|---|---|---|---|
| Time, min | Data | s | Data | s | Data | s | Data | s | Data | s |
| 0.5 | 45.7, 51.3, 28.0 | 12.1 | 19.6, 41.2, 31.6 | 10.8 | 14.7, 21.5, 13.5 | 4.3 | 5.9, 7.8, 4.8 | 1.5 | 2.4, 3.5, 1.6 | 1.0 |
| 1.5 | 72.7, 68.3, 62.0 | 5.4 | 54.4, 54.7, 45.4 | 5.3 | 26.6, 30.1, 23.5 | 3.3 | 14.6, 12.5, 9.0 | 2.8 | 7.2, 6.3, 4.5 | 1.4 |
| 4.0 | 77.1, 73.1, 67.4 | 4.9 | 61.2, 59.6, 52.6 | 4.6 | 34.1, 35.6, 30.9 | 2.4 | 19.7, 15.8, 12.7 | 3.5 | 11.0, 8.5, 5.5 | 2.8 |
| 10.0 | 78.9, 74.0, 71.4 | 3.8 | 63.6, 61.4, 57.4 | 3.1 | 37.2, 38.0, 36.1 | 0.9 | 22.2, 17.9, 16.4 | 3.0 | 13.8, 10.4, 9.1 | 2.4 |
| 16.0 | 79.3, 74.5, 74.6 | 2.7 | 64.4, 62.3, 61.2 | 1.6 | 38.5, 39.3, 39.0 | 0.4 | 23.6, 19.2, 19.6 | 2.4 | 14.2, 11.4, 12.5 | 1.5 |
| 24.0 | 79.6, 74.9, 75.2 | 2.6 | 65.2, 62.8, 62.4 | 1.5 | 39.5, 40.5, 41.1 | 0.8 | 24.8, 20.5, 21.8 | 2.2 | 15.6, 13.2, 14.5 | 1.2 |
| 32.0 | 80.3, 75.2, 75.6 | 2.8 | 65.7, 63.2, 62.9 | 1.5 | 40.3, 41.5, 43.0 | 1.4 | 26.0, 21.7, 23.4 | 2.1 | 16.4, 13.9, 16.1 | 1.4 |

Table A4. Size-by-size recovery data and recovery ranges for the cumulative retained classes, P80 = 300 μm

| | +75 μm | | +150 μm | | +212 μm | | +300 μm | | +355 μm | |
|---|---|---|---|---|---|---|---|---|---|---|
| Time, min | Data | s | Data | s | Data | s | Data | s | Data | s |
| 0.5 | 28.9, 39.5, 22.4 | 8.6 | 18.7, 25.3, 17.3 | 4.3 | 10.1, 15.2, 8.7 | 3.5 | 4.7, 6.4, 3.6 | 1.4 | 2.4, 3.5, 1.6 | 1.0 |
| 1.5 | 51.8, 52.5, 43.7 | 4.9 | 31.5, 34.6, 26.7 | 4.0 | 19.8, 22.0, 15.7 | 3.2 | 12.2, 10.6, 7.6 | 2.3 | 7.2, 6.3, 4.5 | 1.4 |
| 4.0 | 57.1, 57.0, 49.2 | 4.5 | 37.0, 39.1, 32.6 | 3.3 | 26.0, 26.4, 20.8 | 3.1 | 17.1, 13.7, 10.3 | 3.4 | 11.0, 8.5, 5.5 | 2.8 |
| 10.0 | 59.3, 58.4, 53.4 | 3.2 | 40.1, 41.1, 37.1 | 2.1 | 28.9, 28.6, 25.3 | 2.0 | 19.9, 15.9, 14.3 | 2.9 | 13.8, 10.4, 9.1 | 2.4 |
| 16.0 | 60.0, 59.2, 56.5 | 1.8 | 41.9, 42.2, 40.4 | 1.0 | 30.1, 29.9, 28.4 | 0.9 | 21.0, 17.2, 17.9 | 2.0 | 14.2, 11.4, 12.5 | 1.5 |
| 24.0 | 60.7, 59.8, 57.6 | 1.6 | 43.1, 43.2, 42.1 | 0.6 | 31.2, 31.3, 30.5 | 0.4 | 22.3, 18.8, 20.2 | 1.8 | 15.6, 13.2, 14.5 | 1.2 |
| 32.0 | 61.4, 60.3, 58.4 | 1.5 | 44.1, 43.9, 43.4 | 0.3 | 32.1, 32.2, 32.3 | 0.1 | 23.5, 19.9, 22.0 | 1.8 | 16.4, 13.9, 16.1 | 1.4 |

## Appendix B

Tables B1 and B2 summarize the adjusted $R^2$ values obtained with the Gamma model for the conditions with P80 = 212 μm and P80 = 300 μm. These values were sufficiently high for modelling purposes and in almost all cases greater than those obtained with the Single Flotation Rate and Rectangular models. An exception was the retained size class -212/+150 μm at P80 = 300 μm, in which the Rectangular approach led to a higher adjusted $R^2$ of 0.993 than that reported by the Gamma model (0.987).

Table B1. Adjusted $R^2$, Gamma model, retained and cumulative retained classes, condition with P80 = 212 μm

| Gamma Model, P80 = 212 μm | | | |
|---|---|---|---|
| Retained Size Classes | Adjusted $R^2$ | Cumulative Retained Size Classes | Adjusted $R^2$ |
| -150/+75 μm | 0.999 | +75 μm | 0.999 |
| -212/+150 μm | 0.999 | +150 μm | 0.999 |
| -300/+212 μm | 0.998 | +212 μm | 0.998 |
| +300 μm | 0.997 | +300 μm | 0.997 |

Table B2. Adjusted $R^2$, Gamma model, retained and cumulative retained classes, condition with P80 = 300 μm

| Gamma Model, P80 = 300 μm | | | |
|---|---|---|---|
| Retained Size Classes | Adjusted $R^2$ | Cumulative Retained Size Classes | Adjusted $R^2$ |
| -150/+75 μm | 0.985 | +75 μm | 0.983 |
| -212/+150 μm | 0.987 | +150 μm | 0.990 |
| -300/+212 μm | 0.997 | +212 μm | 0.996 |
| -355/+300 μm | 0.992 | +300 μm | 0.993 |
| +355 μm | 0.993 | +355 μm | 0.993 |

## References

AHMED, N., JAMESON, G. J., 1985. *The effect of bubble size on the rate of flotation of fine particles*. Int. J. Miner. Process. 14(3), 195-215.

ALVAREZ-SILVA, M., VINNETT, L., LANGLOIS, R., WATERS, K.E., 2016. *A comparison of the predictability of batch flotation kinetic models*. Miner. Eng. 99, 142-150.

AMINI, E., XIE, W., BRADSHAW, D. J., 2016. *Enhancement of scale up capability on AMIRA P9 flotation model by incorporating turbulence parameters*. Int. J. Miner. Process. 156, 52-61.

BU, X., XIE, G., CHEN, Y., NI, C., 2017(a). *The order of kinetic models in coal fines flotation*. Int. J. Coal Prep. Util. 37(3), 113-123.

BU, X., XIE, G., PENG, Y., GE, L., NI, C., 2017(b). *Kinetics of flotation. Order of process, rate constant distribution and ultimate recovery*. Physicochem. Probl. Miner. Process. 53(1), 342-365.

CRAWFORD, R., RALSTON, J., 1988. *The influence of particle size and contact angle in mineral flotation*. Int. J. Miner. Process. 23, 1-24.

FENG., D., ALDRICH, C., 1999. *Effect of particle size on flotation performance of complex sulphide ores*. Miner. Eng. 12, 721-731.

GARCIA-ZUÑIGA, H., 1935. *Flotation recovery is an exponential function of time.* Bol. Soc. Mac. Min. 47, 83.

GAUDIN, A.M., GROH. J.O., HENDERSON, H.B., 1931. *Effect of particle size in flotation*. Am. Inst. Min. Metall. Eng. Tech. Publ. 414, 3-23.

HARRIS, C.C., CHAKRAVARTI, A., 1970. *Semi-batch flotation kinetics: Species distribution analysis*. Trans. AIME. 247, 162-172.

HUBER-PANU, I., ENE-DANALACHE, E., COJOCARIU, D.G., 1976. *Mathematical models of batch and continuous flotation, Flotation--A. M. Gaudin Memorial*. AIME, Inc., New York, USA, pp. 675-724.

IMAIZUMI, T., INOUE, T., 1963. *Kinetic considerations of froth flotation.* Proc. Sixth Int. Congr. Miner. Process., Cannes, 581-593.

JAMESON, G. J., EMER, C., 2019. *Coarse chalcopyrite recovery in a universal froth flotation machine*. Miner. Eng. 134, 118-133.

KAPUR, P.C., MEHROTRA, S.P., 1973. *Estimation of the flotation rate distributions by numerical inversion of the place transform*. Chem. Eng. Sci. 29, 411-415.

LANGE, A.G., SKINNER, W.M., SMART., R. ST.C., 1997. *Fine: Coarse particle interactions and aggregation in sphalerite flotation*. Miner. Eng. 10, 681-693.

LOTTER, N.O., 1995. *A Quality Control Model for the Development of High-Confidence Flotation Test Data*. University of Cape Town.

POLAT, M., CHANDER, S., 2000. *First-order flotation kinetics models and methods for estimation of the true distribution of flotation rate constants*. Int. J. Miner. Process. 58, 145-166.

POLAT, M., POLAT, H., 2023. *A phenomenological kinetic flotation model: Distinct Time-Variant floatability distributions for the pulp and froth materials*. Miner. Eng. 201, 108217.

TAO, D., 2005. *Role of bubble size in flotation of coarse and fine particles- a review*. Sep. Sci. Technol. 39, 741-760.

TRAHAR, W.J., 1981. *A rational interpretation of the role of particle size in flotation*. Miner. Eng. 8, 289-327.

VINNETT, L., GRAMMATIKOPOULOS, T., EL-MENSHAWY, A.H., WATERS, K.E., 2022. *Justifying size-by-size flotation rate distributions from size-by-association kinetic responses*. Pow. Technol. 395, 168-182.

VINNETT, L., MARION, C., GRAMMATIKOPOULOS, T., WATERS, K.E., 2020. *Analysis of flotation rate distributions to assess erratic performances from size-by-size kinetic tests*. Miner. Eng. 149, 106229.

VINNETT, L., YIANATOS, J., & FLORES, S., 2016. *On the mineral recovery estimation in Cu/Mo flotation plants*. Miner. Metall. Process., 33, 97-106.

VINNETT, L., WATERS, K. E., 2020. *Representation of kinetics models in batch flotation as distributed first-order reactions*. Minerals, 10(10), 913.

WOODBURN, E.T., LOVEDAY, B.K., 1965. *The effect of variable residence time on the performance of a flotation system*. J. South Afr. Inst. Min. Metall. 65, 612-628.

YIANATOS, J., BERGH, L., VINNETT, L., CONTRERAS, F., DIAZ, F., 2010. *Flotation rate distribution in the collection zone of industrial cells*. Miner. Eng. 23, 1030-1035.